Science Advances
AAAS

advances.sciencemag.org/cgi/content/full/4/11/eaav0118/DC1

Supplementary Materials for

Western U.S. lake expansions during Heinrich stadials linked to Pacific Hadley circulation

D. McGee*, E. Moreno-Chamarro, J. Marshall, E. D. Galbraith

*Corresponding author. Email: davidmcg@mit.edu

Published 28 November 2018, *Sci. Adv.* **4**, eaav0118 (2018)
DOI: 10.1126/sciadv.aav0118

This PDF file includes:

Supplementary Materials

Supplementary Text

Estimates of highstand ages for lake basins

We combined recently published highstand age data with the data from a previous compilation of Great Basin highstand ages (*15*). We include only ages that have been published in the peer-reviewed literature, and we only include basins with more than one age on highstand samples or a well-developed lake level curve to test reproducibility. Figure S9 shows data for other terminal basins that were excluded based on these criteria. For basins that overflowed at their highstands and thus have extended periods at the highstand elevation, we have estimated the wettest period during the period of overflow (e.g., Bonneville) or left the overflowing basins out of the compilation and focused on data from terminal basins that received the overflow (e.g., Panamint). All radiocarbon ages are calibrated using INTCAL13, and uncertainties reflect the 95% confidence interval (*64*).

Bonneville Basin

Lake Bonneville overflowed from 18 ka to approximately 15 ka, first from the Bonneville shoreline level and then from the Provo shoreline level after the failure of the threshold lowered the spilling elevation by ~100 m (ref. (*65*)). $\delta^{18}O$ data from lake carbonates suggest that its wettest conditions were prior to 16 ka, as a rapid rise in $\delta^{18}O$ values beginning at 16 ka indicates an increase in water residence time in the basin (*26*, *66*). The disappearance of dense deep-lake carbonate deposition from ~18-16.4 ka offers further support that the wettest (freshest) conditions occurred between 18-16 ka (ref. (*26*)).
Lake Bonneville has a well-documented lake level record spanning 30-10 ka (ref. (*65*)). It reached the Provo shoreline (1450 m) prior to the LGM, and then rose through the LGM before reaching its highstand at 1550 m at around 18 ka. The surface area of the Provo-level lake is 36,923 km^2, while the surface area of the lake its Bonneville shoreline highstand is 50,455 km^2 (ref. (*67*)). The change in surface area from the LGM to the HS1 highstand was thus a factor of <1.4, and was likely closer to 1.1-1.2. This factor provides only a minimum bound on LGM-to-HS1 hydrologic changes, however, because the lake reached its threshold at its highstand shoreline and was no longer able to expand. As a result, Lake Bonneville does not provide a useful estimate of the LGM-to-HS1 increase in surface area.

Chewaucan Basin

Three samples of shorezone tufa (lake carbonate) near the highstand shoreline were radiocarbon dated by Hudson et al. (*25*), producing ages ranging from 14.2±0.2 to 14.6±0.3 cal ka. These authors also present evidence that radiocarbon reservoir effects for the modern and past lake are likely to be negligible. Licciardi (*68*) radiocarbon dated four samples of aquatic gastropod shells associated with shorezone and near-shore deposits and found ages of 13-14 cal ka. These samples came from 30-35 m below the samples of Hudson et al., leading us to use the Hudson et al. results as the best estimate of the deglacial highstand age.

Clover Basin

Munroe and Laabs (*15*) collected five radiocarbon dates from aquatic gastropod shells from highstand beach ridges in the Clover Basin. The two samples from the ridge at the southern end of the basin produce ages of ~19.5 cal ka, suggesting a high lake in the basin for at least a brief portion of the LGM, but at present the lake level curve is not well developed enough to permit estimates of the lake level during the remainder of the LGM. The three samples from the northern end of the basin give a combined age of 17.3±0.2 cal ka, which we take as the best estimate of the age of the deglacial highstand.

Death Valley Basin (Lake Manly)

Death Valley was the terminal basin for the Mojave River during the last glacial period. We do not include dates from the Manix and Mojave basins upstream, as these basins overflowed for long periods of the last glacial maximum and deglaciation (*69*, *70*). Unfortunately, documentation of the deglacial lake level history of the Mojave River drainage's terminal lake in Death Valley (Lake Manly) is poor, relying only on dating of bulk organic matter in basin sediments rather than highstand shoreline sediments, and dates on deep-lake sediments from different cores do not replicate (*71*). As a result, we do not include dates from the Death Valley/Mojave River system in our compilation. We emphasize the need for additional work to constrain lake level histories in the southwestern Great Basin.

Franklin Basin

Munroe and Laabs (*72*) presented five radiocarbon ages on aquatic gastropods from highstand shoreline deposits in the Franklin Basin and several ages on samples from lower shorelines. The highstand ages include one sample that is effectively infinite (>40 ^{14}C ka) and one that falls within the LGM; the authors indicate that both require replication before they can be further interpreted. The remaining three fall during a narrow window within Heinrich Stadial 1 ranging from 15.8±0.2 to 16.4±0.2 cal ka, with the possibility of a brief regression separating the older and younger dates.

The lake level reconstruction of Munroe and Laabs (*72*) indicates that the lake had a surface area of 674 km^2 at the end of the LGM (~19 ka) and a surface area of 1100 km^2 at its HS1 highstand, a factor of 1.67 increase.

Goshute Valley (Lake Waring)

An aquatic gastropod sample from a highstand shoreline ridge from Pleistocene Lake Waring in the Goshute Valley was radiocarbon dated to 16.5±0.3 cal ka (ref. (*15*)). This age overlaps with the age of a highstand sample of 16.7±0.3 cal ka reported by García and Stokes (*73*). We combine these two ages to produce a best estimate of 16.6±0.4 ka for the highstand.

Jakes Basin

García and Stokes (*73*) reported a ^{14}C age of 16.8±0.2 cal ka for an aquatic gastropod sample from the highstand shoreline and a similar age for a result obtained through personal communication from K. Adams. Dating of gastropod samples from two recessional beach ridges just below the highstand shoreline produces ages in stratigraphic order that suggest abandonment of the highstand shoreline by 16.3±0.2 cal ka (ref. (*73*)).

Lahontan Basin

A detailed lake level record for the Lahontan Basin has been developed by Benson et al. (*74*, *75*). Radiocarbon dating of dense tufa coatings and lacustrine gastropods suggest that the lake highstand was attained for a brief period just after 16 cal ka (refs. (*74*, *76*)). A radiocarbon date on a camel bone within a highstand shoreline deposit provides the most precise date of the highstand, indicating that it occurred immediately prior to 15.7±0.2 cal ka (ref. (*76*)).

Lake Lahontan stood at approximately 1265 m during the LGM (*74*), corresponding to a surface area of 14,706 km^2. At its highstand elevation of 1335 m, it had a surface area of 22,776 km^2 (ref. (*77*)), a factor of 1.55 greater than its LGM area.

Mono Basin (Lake Russell)

Radiocarbon dates from shoreline-associated tufas are presented by Benson et al. (*78*), and a later study (*79*) integrates these results with data from sediment deposits in the basin. Both tufa and sediment chronologies suggest a short-lived highstand centered around 15.7±0.2 cal ka (ref. (*15*)).

At present, Mono Lake dissolved inorganic carbon has a radiocarbon reservoir age of approximately 1700 years. Benson et al. (*78*, *79*) assume that reservoir ages were negligible during the lake's highstand

due to greater dilution of volcanic CO_2 inputs and lower DIC concentrations in lake waters. This assumption of a low reservoir age during the highstand is supported by two lines of evidence. First, deglacial sediments from the Mono Basin have been independently dated by magnetic paleosecular variation, with the results suggesting small to negligible radiocarbon reservoir effects (*79*). Second, recent U/Th dating of carbonates near the highstand shoreline has indicated a similar age for the highstand (15.94 ± 0.05 ka, close to the calibrated ^{14}C-based estimate of the highstand age) (*80*). As this age is only available from a thesis at this point, we do not incorporate it into the age estimate in Fig. 1, but it supports a small ^{14}C reservoir age at this time.

The lake level record of Benson et al. (*78*) indicates that Lake Russell was at or near 2035 m elevation during the LGM, corresponding to a surface area of 435 km^2. At its HS1 highstand level of 2155 m, it had a surface area of 790 km^2, representing a factor of 1.82 increase (*78*).

Panamint Basin

The Panamint Basin was the terminal basin in the Owens River system during the pluvial maximum of the last deglaciation (*81*), so we focus on lake level changes in this basin rather than overflowing basins upstream (Owens, China, Searles) or downstream (Death Valley). Lake levels in the basin are poorly documented, highlighting the need for additional work to date overflow from Searles Basin and water fluctuations in Panamint Basin. Jayko et al. (*81*) dated tufa and lacustrine shells from nearshore deposits in the Panamint Basin. Though LGM results are scattered, with dated samples spanning ~150 m and no replication of ages, deposits located near to each other in elevation and space give overlapping ages of 17.0±0.3 cal ka and 17.2±0.3 cal ka for the highest lake levels during the deglaciation.

Surprise Basin

A detailed hydrograph for the LGM and deglacial history of Lake Surprise was developed by Ibarra et al. (*6*). The authors determined that a tufa sample ^{14}C-dated to 15.2±0.2 cal ka provides the best estimate of the highstand age, and additional ^{14}C dates suggest sustained regression of the lake after this time. We use this estimate for the highstand age here, but we also note that U-Th and ^{14}C dates from the earlier portion of the deglaciation present an unclear picture of the lake history between ~18-15.2 ka, suggesting a need for further work to determine the duration of the highstand.

Shoreline data from Lake Surprise indicate that the lake elevation was ~1420-1440 m during the LGM, corresponding to surface areas of 851-977 km^2. At its HS1 highstand of 1531 m, the lake had a surface area of 1366 km^2, a factor of 1.49 larger than the average LGM lake area (*6*).

Thompson Basin

Beach deposits at the elevation of the most recent highstand in the shallow Thompson Basin (southwestern California) were studied by Orme (*82*). Dating of bulk organic matter from cores produces a broad range of ages from the uppermost beach deposits: 7.66±0.08 cal ka, 12.64±0.08 cal ka, 12.69±0.06 cal ka, and 15.8±0.2 cal ka. This wide range may reflect contamination of bulk organic matter by younger soil organic matter or detrital organic matter. The lack of agreement between dates on highstand deposits leads us to leave this basin's data out of the quality-controlled dataset in Fig. 1.

Sensitivity tests for lake water budget estimates

Here we evaluate the importance of two assumptions made in the water budget estimates provided in the main text. First, we assumed that E_L=*PET*. E_L and *PET* may differ in that many ways of calculating *PET* incorporate the conductance of water through vegetation. For example, E_L as estimated by the Penman equation (*83*) ($E_{L,Penman}$) and *PET* estimated by the Penman-Monteith equation (*84*) ($PET_{P\text{-}M}$) (commonly used expressions for evaporation from lakes and potential evapotranspiration from vegetated surfaces, respectively) differ by a factor of

$$\frac{E_{L,Penman}}{PET_{P-M}} = \frac{\Delta + \gamma\left(1 + \frac{C_{at}}{C_{can}}\right)}{\Delta + \gamma} \quad \text{(S1)}$$

where Δ is the slope of saturation vapor pressure as a function of temperature (~0.08 at 10˚C, taking this as the mean annual temperature in the Great Basin at the LGM), γ is the psychrometric constant (~0.06), C_{at} is atmospheric conductance (primarily a function of wind speed), and C_{can} is canopy conductance (primarily a function of vegetation type.) Using typical values for grasslands (*49*) suggests E_L/PET ~1.5, consistent with studies suggesting that the Penman equation is accurate for annual mean lake evaporation (*85*) but may overestimate evapotranspiration from vegetated surfaces by tens of percent (*86*). To test the importance of the assumption that $PET=E_L$, we calculated lake area changes with E_L equal to PET*1.5 (representing $PET< E_L$ due to low water vapor conductance by vegetation.) This substantial change in E_L/PET ratios produces only ~2-10% reductions in A_{L2}/A_{L1} for a given value of P_2/P_1 relative to $PET=E_L$, with increasing differences with increasing P_2/P_1 (fig. S10).

We also evaluate the influence of a decline in E_L in response to hosing. Figure S10 shows the influence of a 5% decrease in evaporation on lake areas (i.e., $E_{L2}= 0.95*E_{L1}$) across a wide range of precipitation changes. As discussed in the main text, even this small value may substantially overestimate LGM-to-HS1 evaporation changes. As expected, decreased evaporation increases lake areas; the combination of increased precipitation and reduced evaporation in our Strong simulation brings the simulated lake areas into the range of observed LGM-to-HS1 lake area changes, while the responses in the Weak simulation and TraCE-21ka remain much smaller than the observed changes. Changing *PET* in response to hosing has negligible impact on the simulated lake area response.

Further notes on the Budyko framework

We note that equation (2) in the main text is a restatement of the "Fu Equation" (*87*) as referenced by (*88*).

Tropical Pacific vs. tropical Atlantic drivers of Aleutian Low response

Okumura et al. (*24*) found that the wintertime Aleutian Low consistently deepened in response to hosing in a comparison of simulations with four different fully coupled climate model simulations. Analyzing one model's response (CCSM2), they found that greater Aleutian Low deepening was associated with warmer before-hosing sea-surface temperatures in the tropical western North Atlantic; they thus suggested that the deepening of the Aleutian Low results primarily from anomalous propagation of Rossby waves from decreased atmospheric deep convection in the western tropical North Atlantic due to the hosing. Our results, however, do not fully support the proposed atmospheric bridge. The greatest deepening of the Aleutian Low occurs in the Strong simulation, which exhibits generally colder tropics than the Weak simulation in both the control and hosed experiments and shows smaller precipitation reductions in the Caribbean Sea in response to hosing. Further, our analysis emphasizes the importance of the southeastward shift of the Aleutian Low in addition to its overall deepening, as this shift draws southwesterly moisture transport into the southwestern U.S. rather than farther northwest. The Aleutian Low response in the CCSM2 results shown by Okumura et al. shows no evidence for a shift, as pressure anomalies are centered in the central North Pacific rather than the northeast Pacific (*24*). It is unknown how the central Pacific Hadley circulation varied in the experiments in Okamura et al., and whether it agrees with our proposed mechanism; future work should investigate this response in hosing experiments conducted with different models.

Supplementary Table

Table S1. Lake highstand ages used in Fig. 1.

Basin (Lake name)	^{14}C age (yrs BP)	± (1σ)	Calendar age (yrs BP)	95% CI (+)	95% CI (-)	References
Bonneville[1]			17000	18000	16000	(*26*, *65*, *66*)
Clover[2]	14228	71	17324	17550	17090	(*15*)
Goshute (Waring)	13800	50	16694	16945	16450	(*73*)
	13650	75	16458	16767	16210	(*15*)
Franklin	13150	55	15798	16022	15583	(*72*)
	13250	55	15929	16124	15730	
	13600	45	16384	16605	16200	
Mono (Russell)	13100	50	15721	15955	15465	(*15*, *78*, *79*)
Panamint	13970	80	16970	17254	16620	(*81*)
	14130	90	17197	17495	16896	
Jakes	13870	50	16801	17023	16554	(*73*)
Lahontan	13070	60	15667	15906	15370	(*89*)
Surprise	12750	50	15200	15380	15020	(*6*)
Chewaucan	12260	40	14163	14371	14014	(*25*)
	12270	40	14177	14416	14027	
	12440	40	14559	14906	14231	

[1]Midpoint between approximate age for reaching highstand (~18 ka) and onset of increasing trend in δ^{18}O in lake carbonates (~16 ka).
[2]Three overlapping ^{14}C ages combined by authors.

Supplementary Figures

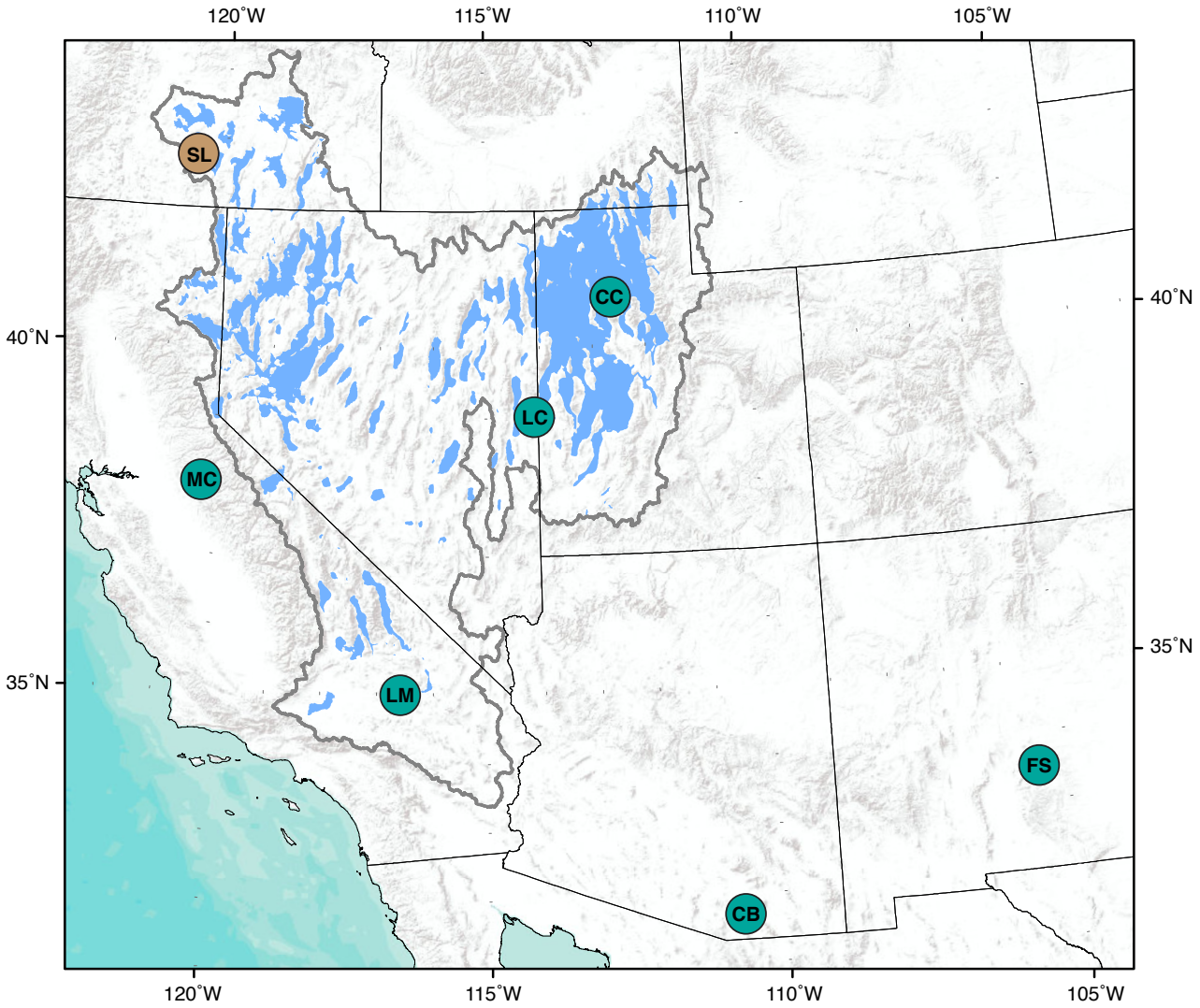

Fig. S1. Well-dated proxy evidence of hydrologic changes during Heinrich stadials before the LGM. Green circles indicate sites with evidence for shifts to wetter conditions and/or greater winter precipitation during Heinrich stadials; the brown circle indicates a site with evidence for shifts to drier conditions. Grey line is the outline of the Great Basin, and blue shading indicates the areas of paleolakes at their maximum extents during the last glacial period and deglaciation. FS: Fort Stanton Cave speleothem $\delta^{18}O$ record (HS2-5, other stadials) (*19*); CB: Cave of the Bells speleothem $\delta^{18}O$ record (HS4, other stadials) (*22*); LM: Lake Manix sediments (HS3-4, other stadials) (*27*); CC: Cathedral Cave carbonate reflecting Lake Bonneville $\delta^{18}O$ and $\delta^{234}U$ (HS2) (*26*); LC: Lehman Cave speleothem Mg/Ca and Sr/Ca records (HS11) (*28*); MC: McLean's Cave Mg/Ca, Sr/Ca, $\delta^{13}C$, $^{87}Sr/^{86}Sr$ and reflectance record (HS6) (*29*); SL: Summer Lake/Chewaucan Basin sediment record (H2-5, other stadials) (*30*).

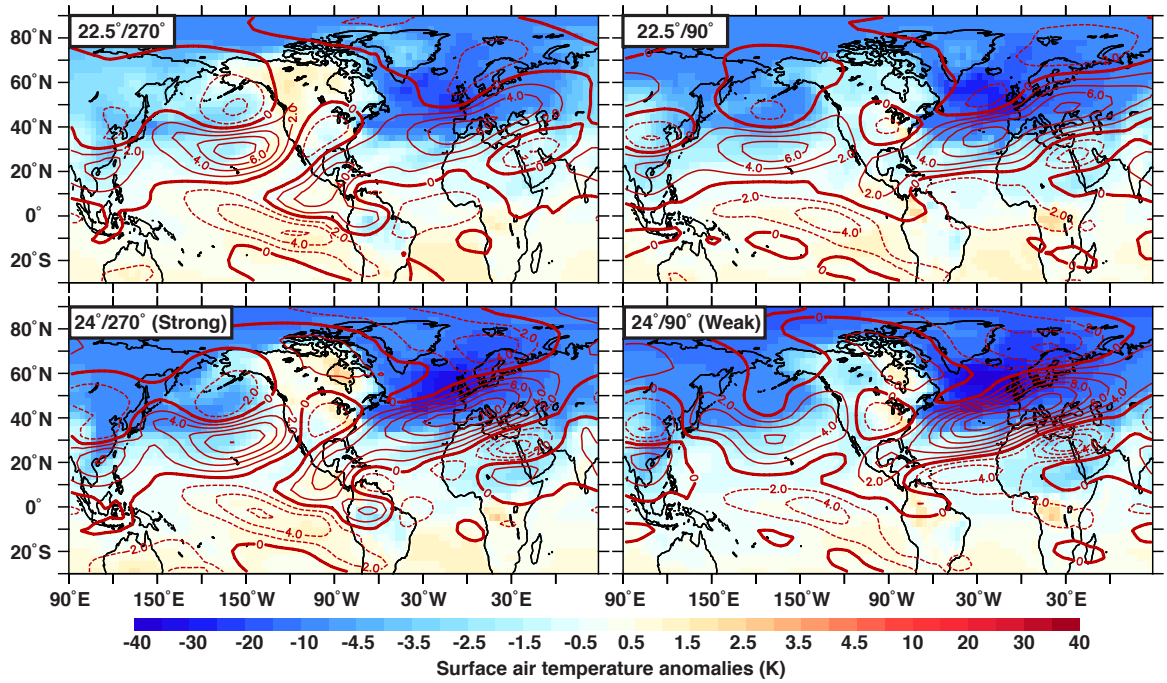

Fig. S2. Temperature and wind anomalies in each hosing experiment. Anomalies in the DJF near-surface (2 m) temperature (K; shading), and 300 hPa zonal wind (m/s; contours) between each hosing experiment and its corresponding control are shown. The Strong and Weak simulations discussed in the main text are also labeled. Note that the color scale is nonlinear to allow a better view of the values over western North America.

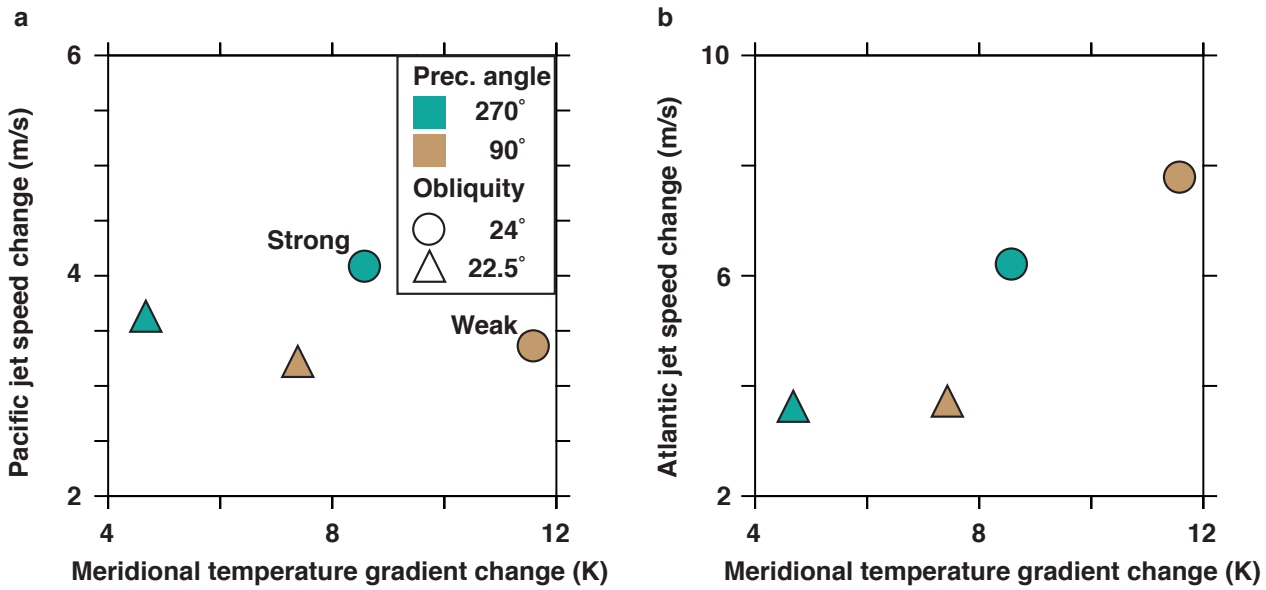

Fig. S3. Relationship between jet changes and meridional temperature gradient changes. Scatter plot of the change between the hosing and control experiments in the DJF NH **a)** Pacific and **b)** Atlantic jet stream versus the corresponding change in the DJF NH meridional temperature gradient. Brown symbols indicate simulations with 90˚ precession angle; green symbols indicate simulations with 270˚ precession angle; triangles and circles indicate 22.5˚ and 24˚ obliquity, respectively. The Pacific and Atlantic jets (in m/s) are defined as the maxima of the zonal wind at 300 hPa, averaged between 150°E and 140°W and between 80°W and 30°E respectively. The meridional temperature gradient is the difference in the zonally averaged global DJF surface air temperature between the Tropics (averaged between 30°S and 30°N) and NH high latitudes (between 60°N and 90°N). Note that the Atlantic jet becomes stronger as the meridional temperature gradient increases, but there is no clear relationship between the meridional temperature gradient and the Pacific jet. The Strong and Weak simulations discussed in the main text are labeled in the left panel.

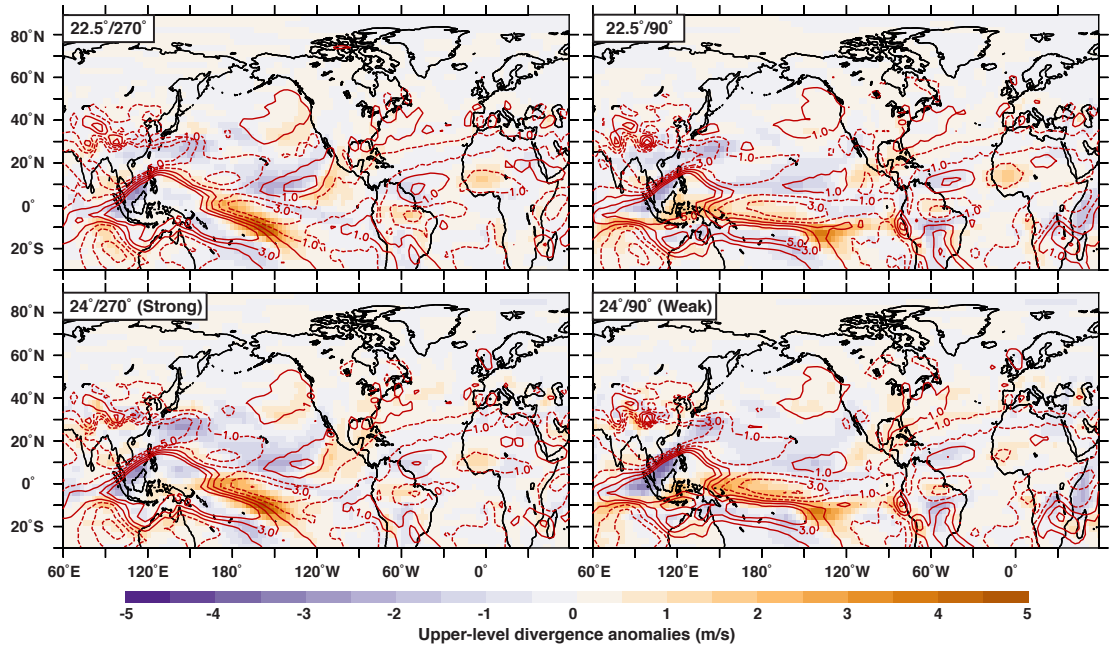

Fig. S4. Anomalies of upper-level divergence in response to hosing. Upper-level (~150 hPa) DJF divergence anomalies are shown by shading, with positive values indicating anomalous divergence and negative values indicating anomalous convergence; units are m/s. Contours (m/s) show the mean DJF divergence in the respective glacial control simulations. All values are scaled by a factor of 10^6. Note the greater anomalous convergence in the subtropical central Pacific (centered at 20˚N, 150˚W) in the Strong simulation than in the Weak simulation associated with the greater central Pacific Hadley circulation intensification in the Strong simulation, driving the larger jet and Aleutian Low responses observed.

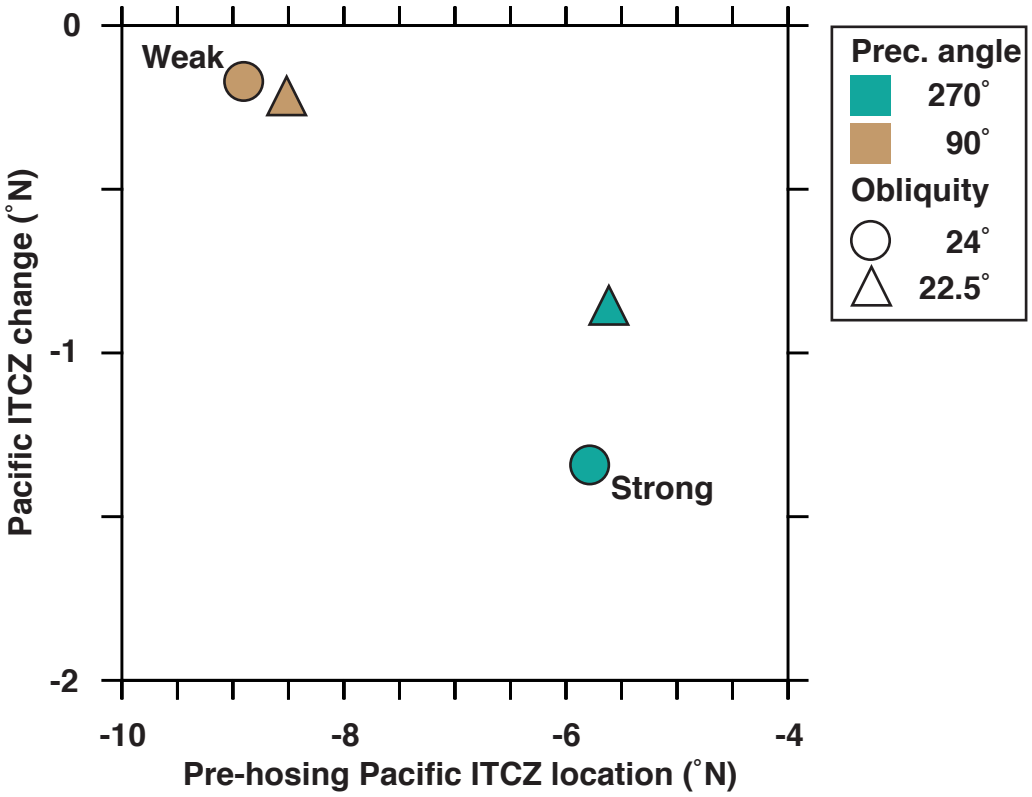

Fig. S5. Comparison of central Pacific DJF ITCZ shift in response to hosing to its position in the corresponding glacial control simulation. The ITCZ position is defined as described in the Methods. Brown symbols indicate simulations with 90˚ precession angle; green symbols indicate simulations with 270˚ precession angle; triangles and circles indicate 22.5˚ and 24˚ obliquity, respectively. The Strong and Weak simulations discussed in the main text are labeled. Note that the simulations in which the ITCZ begins farther north show a larger response to hosing.

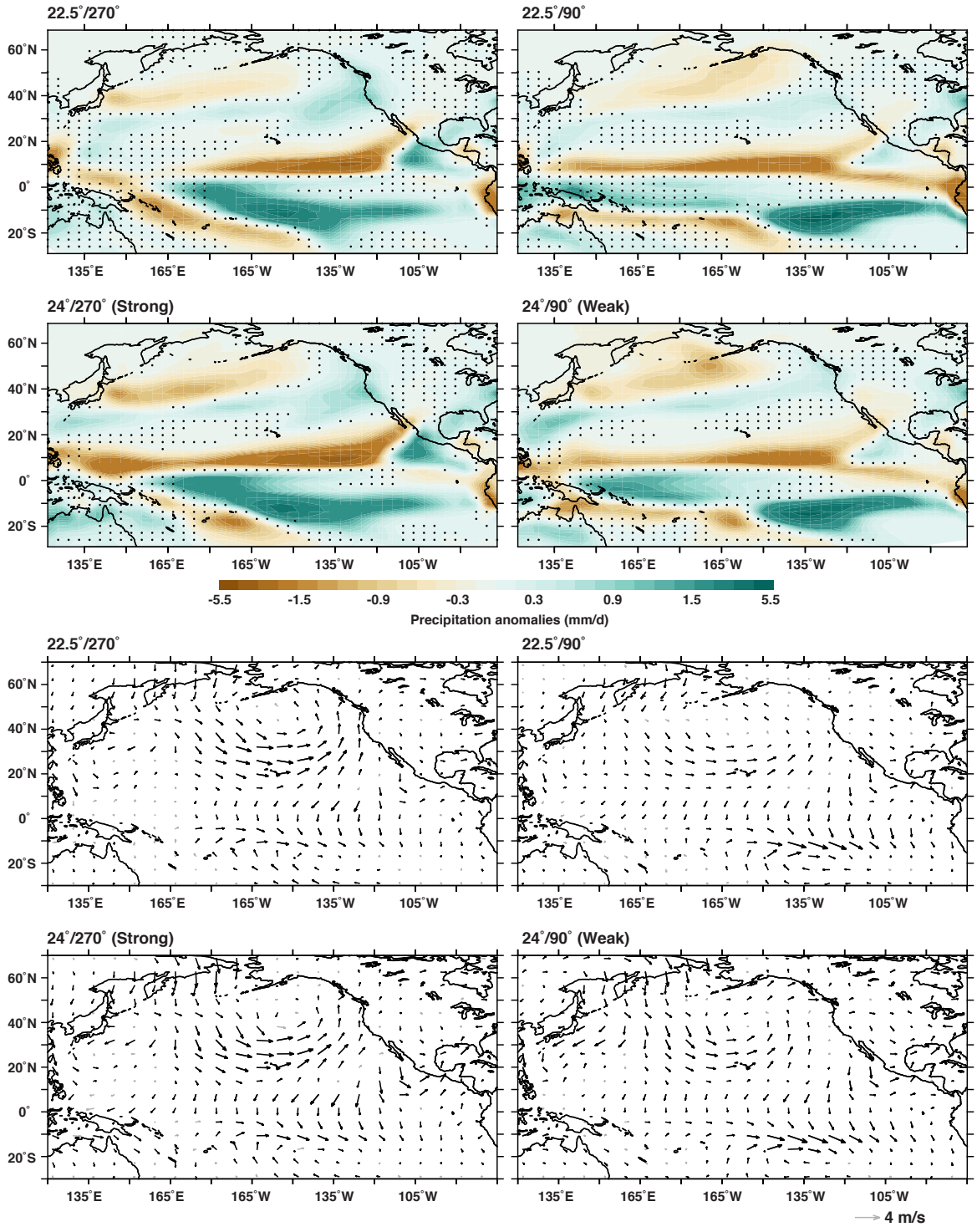

Fig. S6. DJF precipitation and wind anomalies for all four hosing experiments. DJF precipitation anomalies (top panels) and near-surface (10 m) wind anomalies (bottom panels) for all four hosing experiments. Each panel is labeled with the obliquity (22.5˚ vs. 24˚) and precession angle (90˚, for perihelion in austral summer, vs. 270˚, for perihelion in boreal summer) used for the respective simulation. The Strong and Weak simulations discussed in the main text are also labeled. Stippling (top panels) and grey vectors (bottom panels) indicate regions in which precipitation changes are not significant at the 5% level (Methods).

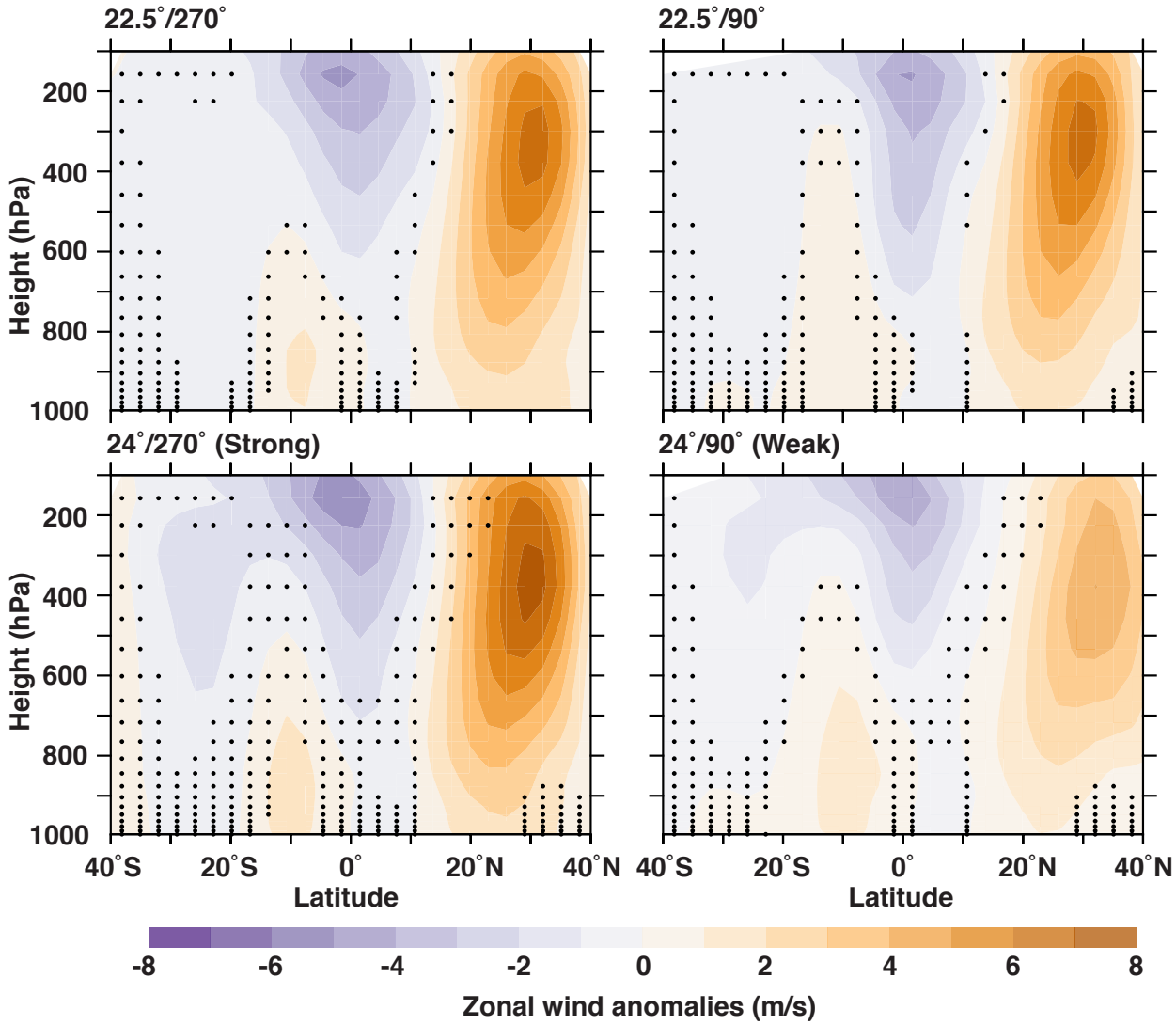

Fig. S7. DJF central Pacific zonal wind anomalies for all four hosing experiments. Each panel is labeled with the obliquity (22.5˚ vs. 24˚) and precession angle (90˚, for perihelion in austral summer, vs. 270˚, for perihelion in boreal summer) used for the respective simulation. The Strong and Weak simulations discussed in the main text are also labeled. Stippling indicates regions in which wind changes are not significant at the 5% level (Methods).

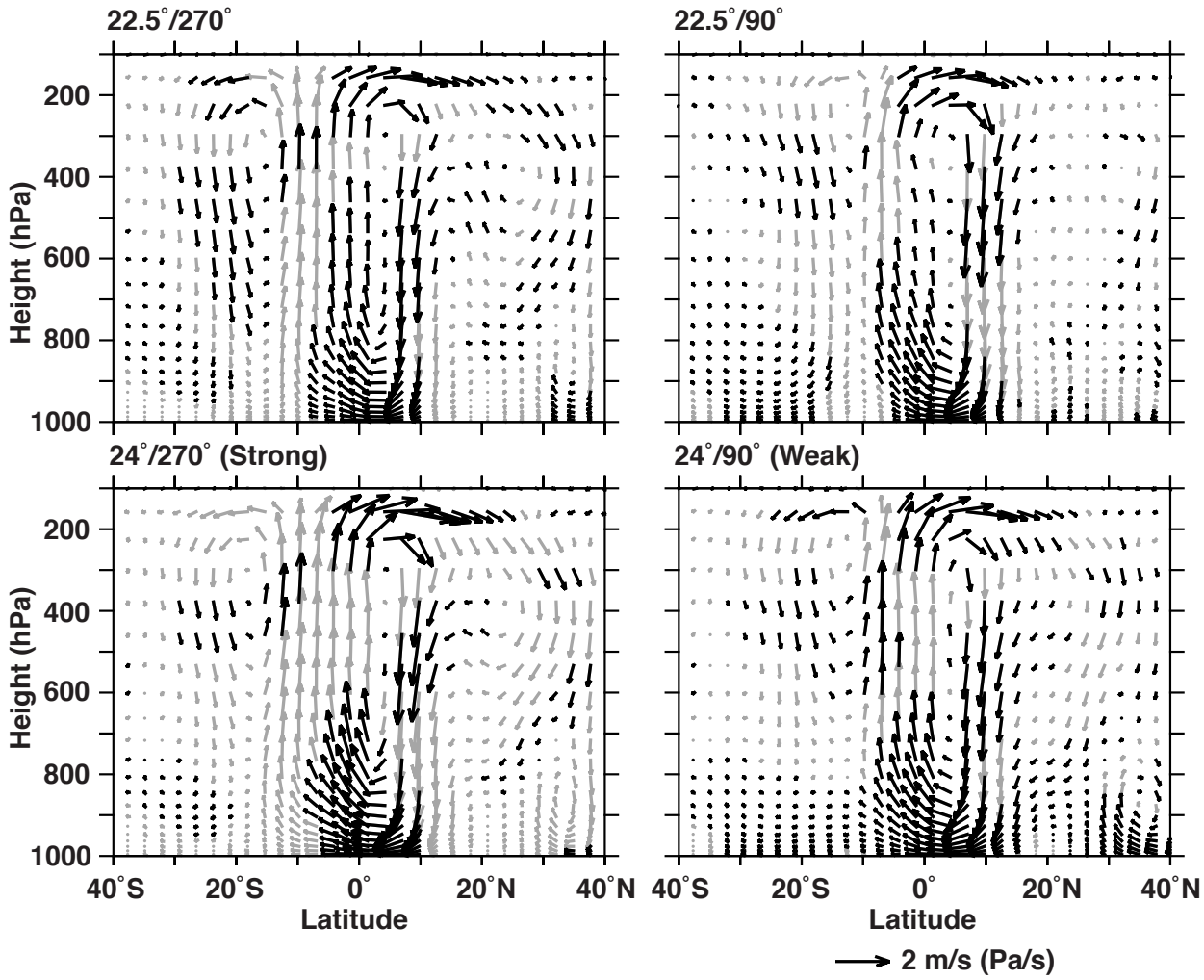

Fig. S8. DJF central Pacific circulation anomalies for all four hosing experiments. Vectors indicate anomalies in the divergent wind and isobaric vertical velocity (vectors, in m/s and Pa/s respectively). Each panel is labeled with the obliquity (22.5˚ vs. 24˚) and precession angle (90˚, for perihelion in austral summer, vs. 270˚, for perihelion in boreal summer) used for the respective simulation. The Strong and Weak simulations discussed in the main text are also labeled. Grey vectors indicate regions in which meridional divergent wind changes are not significant at the 5% level (Methods). Significance cannot be calculated for the vertical component of the winds, as 5-daily data were not saved, but we expect that significant meridional anomalies in the upper and lower branches of the anomalous Hadley circulation (as shown) would be accompanied by significant vertical anomalies in the ascending and descending limbs.

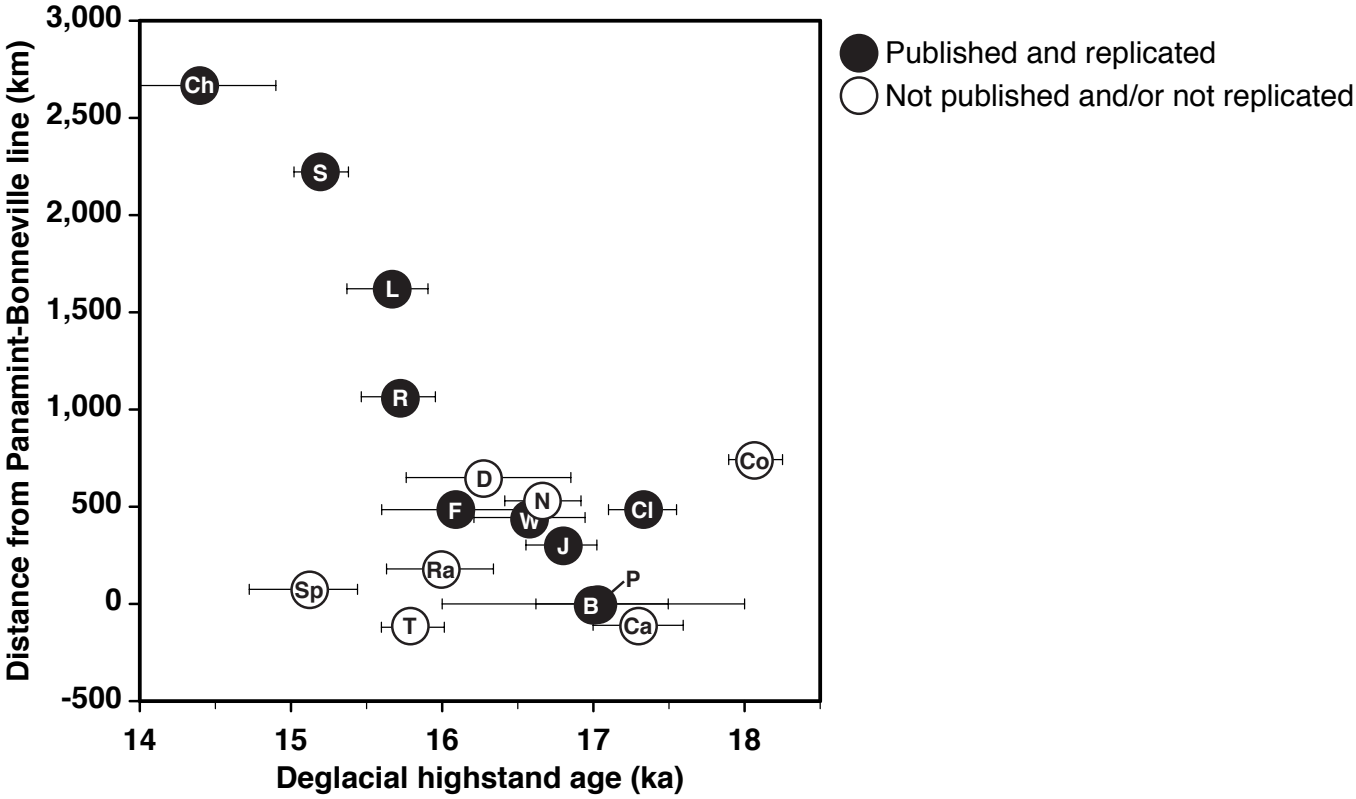

Fig. S9. Ages of terminal lake highstands in the U.S. Great Basin during the last deglaciation, including ages excluded by quality control criteria. Age estimates with 95% confidence intervals for wettest conditions during the deglaciation in each basin as a function of distance from a line connecting the Panamint and Bonneville basins (dashed line in Fig. 1a). Filled symbols are identical to Fig. 1b; white circles are highstand ages that do not pass quality-control criteria (i.e., have not been published in peer-reviewed literature and/or have not been replicated.) Paleolakes: B: Bonneville; Ca: Carpenter (*90*); Ch: Chewaucan; Cl: Clover; Co: Columbus (*91*); D: Diamond (*92*); F: Franklin; J: Jakes; L: Lahontan; N: Newark (*91*); P: Panamint; R: Russell; Ra: Railroad (*90*); S: Surprise; Sp: Spring (*90*); T: Thompson (*82*); W: Waring. See Table S1 and the Supplementary Text for further information and references.

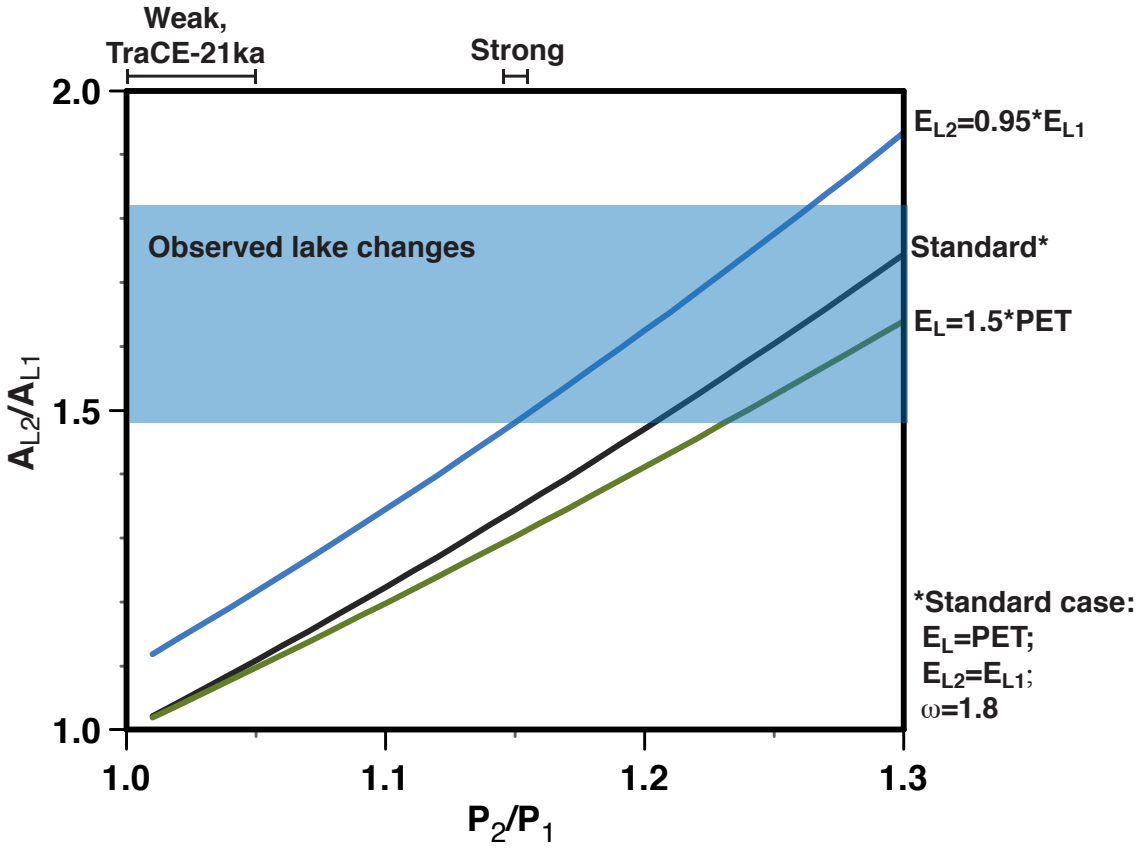

Fig. S10. Simulated lake area changes (A_{L2}/A_{L1}) in response to precipitation changes (P_2/P_1), evaporation changes, and differences in PET/E_L. The black line ("Standard") corresponds to ω =1.8, PET/P_1 = 1.5, PET=E_L, and no change in lake evaporation. The blue line uses the same values of ω=1.8 and PET/P_1 and includes a 5% decrease in lake evaporation (no change is made in PET.) The green line explores the impact of E_L =1.5**PET*, with all other variables the same as the Standard case. Bars at the top indicate precipitation changes in our Strong and Weak hosing simulations and between the LGM and HS1 in the TraCE-21ka experiment. The blue region indicates reconstructed lake area changes between the LGM and HS1.